DeeplsoFun: A deep domain adaptation approach to predict isoform functions

Dipan Shaw 1, *, Hao Chen 1 and Tao Jiang 1, 2, *

Abstract

Motivation: Isoforms are mRNAs produced from the same gene locus by alternative splicing and may have different functions. Although gene functions have been studied extensively, little is known about the specific functions of isoforms. Recently, some computational approaches based on multiple instance learning have been proposed to predict isoform functions from annotated gene functions and expression data, but their performance is far from being desirable primarily due to the lack of labeled training data. To improve the performance on this problem, we propose a novel deep learning method, DeeplsoFun, that combines multiple instance learning with domain adaptation. The latter technique helps to transfer the knowledge of gene functions to the prediction of isoform functions and provides additional labeled training data. Our model is trained on a deep neural network architecture so that it can adapt to different expression distributions associated with different gene ontology terms.

Results: We evaluated the performance of DeeplsoFun on three expression datasets of human and mouse collected from SRA studies at different times. On each dataset, DeeplsoFun performed significantly better than the existing methods. In terms of area under the receiver operating characteristics curve (or AUC), our method acquired at least 26% improvement and in terms of area under the precision-recall curve (or AUPRC), it acquired at least 10% improvement over the state-of-the-art methods. In addition, we also study the divergence of the functions predicted by our method for isoforms from the same gene and the overall correlation between expression similarity and the similarity of predicted functions.

Availability: https://github.com/dls03/DeeplsoFun/

1 Introduction

In eukaryotes, the mechanism of alternative splicing produces multiple isoforms from the same gene. Studies in (Pan et al., 2008; Wang et al., 2008) reveal that more than 95% of human multi-exon genes undergo alternative splicing. Though the changes in the sequences of the isoforms of the same gene are very small, they may have a systematic impact on cell functions and regulation (Gallego-Paez et al., 2017). It has been widely reported that isoforms from the same gene sometimes have distinct or even opposite functions (Himeji et al., 2002; Melamud and Moult, 2009; Mittendorf et al., 2012). For example, among the two isoforms, *I-KICpo* and *s-KICpo*, of gene *KIHEM13* that use different transcription start sites, only *s-KICpo* is involved in the growth of *K. lactis* $\Delta hem13$ mutants (Vázquez et al., 2011). There is also evidence that alternative splicing plays an important role in the evolutionary process (Gueroussov et al., 2015). For example, the absence of exon 9 in one of the isoforms of gene *PTBP1* expressed in the brains of mammals amplifies the evolutionary difference between

mammals and the other vertebrates (Gueroussov et al., 2015). Many studies have found that alternative splicing is critical in human health and diseases. For example, to escape from cell death in tumorigenesis, gene BCL2LI produces two isoforms with opposite functions, where BCL-XS is pro-apoptosis but BCL-XL is anti-apoptosis (Revil et al., 2007). Similarly, gene CASP3 has two isoforms, with CASP3-L being pro-apoptosis and CASP3-S anti-apoptosis (Végran et al., 2006). An isoform of gene TNR6 that skips exon 6 may initiate cell death (Bouillet and O'reilly, 2009). Among the two isoforms of gene PKM, PKM1 and PKM2 that skip exons 9 and 10 respectively, only PKM2 is widely expressed in cancer cells (Mazurek et al., 2005). Besides these examples, the results in (Himeji et al., 2002; Melamud and Moult, 2009; Oberwinkler et al., 2005; Pickrell et al., 2010) offer more interesting stories of isoforms with dissimilar functions and hence motivate the study of specific functions of isoforms.

There is rich literature concerning the prediction of gene functions (Barutcuoglu et al., 2006; Mi et al., 2012; Schietgat et al., 2010; Vinayagam et al., 2004; Yang et al., 2015). In particular, the UniProt Gene Ontology (GO) database has been widely used as a standard reference for gene function annotation (Ashburner et al., 2000; Barrell et al., 2008). It is organized as a directed acyclic graph (DAG) where the nodes represent functional

1

¹Department of Computer Science and Engineering, University of California, Riverside, CA and

²Bioinformatics Division, BNRIST / Department of Computer Science and Technology, Tsinghua University, Beijing, China

^{*}To whom correspondence should be addressed.

terms (referred to as GO terms) and edges indicate how a term is subdivided into more detailed functional concepts. The DAG is comprised of three main branches, i.e., Biological Process (BP), Molecular Function (MF) and Cellular Component (CC) (Ashburner et al., 2000), representing three distinct classes of functional concepts. The functions of a gene are then represented by mapping the gene to all relevant terms in GO. In contrast, very little systematic study has been done about the specific functions of isoforms and there is no central database that provides annotated isoform functions. Recently, several machine learning approaches were proposed to predict isoform functions from GO and RNA-Seq expression data (Eksi et al., 2013; Li et al., 2013, 2015; Luo et al., 2017; Panwar et al., 2016). In other words, these methods attempt to distribute the annotated functions of a gene to its isoforms based on their expression profiles. Since labeled training data were generally unavailable, Eksi et al. (2013) (see also Panwar et al. (2016)), Li et al. (2013) and Luo et al. (2017) solved the problem by using a semi-supervised learning technique called multiple instance learning (MIL). However, the experimental performance of their methods was quite poor. For example, on their respective datasets, the best areas under the receiver operating characteristics curve (or AUCs) achieved by the methods were only 0.681, 0.671 and 0.677, respectively. We believe that a primary cause of the poor performance was due to the lack of labeled training data.

In this paper, we propose a novel method, DeepIsoFun, for predicting isoform functions from GO and RNA-Seq expression data. It directly addresses the challenge from the lack of labeled training data by combining MIL with the domain adaptation (DA) technique. The two techniques are somewhat complementary to each other since while MIL takes advantage of the gene-isoform relationship, DA helps to transfer the existing knowledge of gene functions to the prediction of isoform functions. More precisely, we consider each gene as a bag and each isoform as an instance in the context of MIL where the labels (i.e., functions) of the instances in each bag are given as a set (Dietterich et al., 1997). The goal of MIL is to assign the labels (i.e., functions) of each bag (i.e., gene) to its instances (i.e., isoforms) with the constraint that each label is assigned to at least one instance in the bag and no instance is assigned a label that does not belong to its bag (Andrews et al., 2003; Wang et al., 2017). To apply the DA technique, we take advantage of the fact that genes actually have expression data and thus can be considered as instances in another domain (i.e., the gene domain). In other words, a gene can be regarded as both an instance in the gene domain as well as a bag in the isoform domain. Since gene functions are known in GO, the DA technique can be used to transfer knowledge (i.e., the relationship between expression and function) from the gene domain (called the source domain) into the isoform domain (called the target domain) (Ganin and Lempitsky, 2015; Long et al., 2015; Pan et al., 2011; Tzeng et al., 2014). Hence, the gene domain helps provide the much needed labeled training data.

The model of DeepIsoFun consists of three classifiers. The first attempts to correctly label the functions of each gene. The second attempts to correctly label the functions of each isoform (via bags). The third tries to make sure that instances from the source and target domains are indistinguishable so knowledge can be transferred. To implement the model, we use a neural network (NN) auto-encoder to extract features from expression data that are both domain-invariant and discriminative for functional prediction, inspired by the work in (Ajakan et al., 2014; Ganin and Lempitsky, 2015). The three classifiers are also implemented as parallel NNs and connected to the auto-encoder NN to form a deep feed-forward network. The NNs involve mostly standard hidden layers and loss functions and can be trained for each GO term sequentially using a standard back-propagation algorithm based on stochastic gradient descent, but we also incorporated the gradient reversal layer to facilitate the DA method as introduced in (Ganin and Lempitsky, 2015) and take advantage of the hierarchical structure of GO in training. In particular, we traverse GO starting at the leaf

nodes and make sure that the model is trained for all child nodes before it is trained for a parent node so the training for the parent node can benefit from earlier trainings. This also helps maintain the prediction consistency throughout GO.

To evaluate the performance of DeepIsoFun, we use three RNA-Seq expression datasets of human and mouse collected from the NCBI Reference Sequence Archive (SRA) at different times. The first is a new (also the largest) dataset that we extracted from the SRA recently. The other two were studied in (Eksi et al., 2013; Li et al., 2013). To measure the prediction accuracy, we use both AUC and area under the precision recall curve (AUPRC) against specific baselines (measured at the gene level, as done in (Eksi et al., 2013; Li et al., 2013; Luo et al., 2017)). Our experimental results consist of two parts. In the first part, we analyze various properties of DeepIsoFun such as the effect of domain adaptation on its performance, impact of the frequency of a GO term in genes on its performance, difference in performance across the three main branches of GO, divergence of the functions predicted for the isoforms of a gene, and correlation between the similarity of expression profiles and the similarity of predicted functions. In the second part, we compare the performance of DeepIsoFun with the methods introduced in (Eksi et al., 2013; Li et al., 2013; Luo et al., 2017; Panwar et al., 2016), mi-SVM, iMILP and WLRM, based on support vector machines (SVMs), label propagation and weighted logistic regression, respectively. On our new dataset, DeepIsoFun outperformed these mi-SVM, iMILP and WLRM methods by 31%, 64% and 23% (against baseline 0.5) in AUC, respectively. In terms of AUPRC, DeepIsoFun outperformed them by 59%, 11% and 63%, respectively, against baseline 0.1. Similar improvements on the other two datasets were also observed. We believe that besides the deep learning framework, the DA technique also played an important role in these significant improvements

The rest of the paper is organized as follows. In the Method section, we describe the proposed method and its NN implementation in more detail. The section of Experimental evaluation shows how to determine the key parameters in the NN, the construction of experimental datasets and all computational results on these datasets. Some possible future work is briefly outlined in the Discussion section.

2 Method

In this section, we detail our proposed method, DeepIsoFun, for predicting isoform functions from GO and RNA-Seq data. As outlined above, our learning framework consists of two domains, the gene domain (denoted as $y_d=0$) and the isoform domain (denoted as $y_d=1$), where y_d represents a domain class label. In the isoform domain, the isoforms of each gene form a bag in the context of MIL. The gene domain will be considered as the source domain and the isoform domain as the target domain in the context of DA. Suppose that there are n genes and m isoforms. Hence, the isoforms are divided into n bags in the isoform domain. Suppose that the expression profiles consists of r experiments.

Given a GO term, the data in the gene (or source) domain is denoted as a pair (x_s,y_s) , where x_s is an $n\times r$ feature matrix representing the expression profiles of all n genes over the r experiments and y_s is an n-dimensional binary vector (called gene class labels) indicating whether each gene has the functional term or not. Similarly, the data in the isoform (or target) domain is denoted as a pair (x_t,y_t) , where x_t is an $m\times r$ feature matrix representing the expression profile of all isoforms and y_t is an m-dimensional binary vector (called isoform class labels) indicating whether each isoform domain is also denoted as a pair (X_T,Y_T) , where X_T is a binary matrix representing the membership of isoforms in each bag (or gene) and Y_T is an n-dimensional binary vector (called bag class labels) indicating whether the isoforms in each bag collectively have the functional term or not. Observe that $Y_T = y_s$.

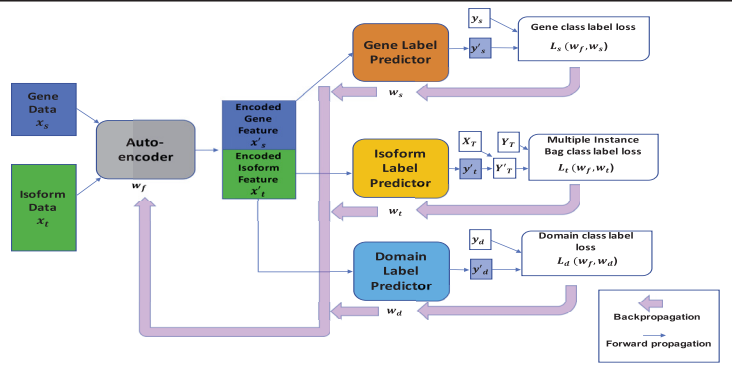


Figure 1: The proposed NN architecture. It includes an auto-encoder (gray), a gene class label predictor (orange), an isoform class label predictor (yellow), and a domain label predictor (blue). These four modules jointly form a feed-forward NN, where the auto-encoder consists of two hidden layers and other three components consist of one hidden layer each. The NN is trained using a standard cross-validation so that the auto-encoder extracts features from the input expression profiles to minimize the loss in gene class label prediction loss, minimize the loss in bag class label prediction and maximize the loss in domain classification so that knowledge can be transferred from the gene domain to the isoform domain. In the figure, the rectangle boxes represent the input data and extracted features. Particularly, x_s is the input gene expression data, x_t is the input isoform expression data, x_s' the encoded gene feature data, and x'_t the encoded isoform feature data. Each variable y'_s , y'_t and y'_d represents a predicted gene class label vector, a predicted isoform class label vector and a predicted domain class label vector, respectively. The notation y_s represents the true gene class label vector that is used to calculate L_s , i.e., gene class label loss. The notation X_T represents the membership of isoforms in the bags and $Y_T = y_s$ is the true bag class label vector that is used to calculate L_t , i.e., bag class label loss via a multiple instance loss procedure. The notation y_d is the true domain class label vector that is used for calculating L_d , i.e., domain class label loss. Forward arrows represent forward propagation and backward arrows show how losses are backpropagated to allow for the adjustment of the weights w_f, w_s, w_t , and w_d used in the auto-encoder, gene class label predictor, isoform class label predictor, and domain label predictor, respectively.

As mentioned above, our method combines the MIL and DA techniques and uses three classifiers to classify isoforms with respect to each GO term. It is implemented on a deep NN architecture with four modules: an autoencoder, a gene function predictor in the gene domain, an isoform function predictor in the isoform domain, and a domain label predictor, as illustrated in Figure 1. The input gene and isoform expression features (x_s and x_t) are mapped by the auto-encoder to obtain an encoded feature matrix x_f . We denote the training weights used in this mapping as w_f .

Our goal for the auto-encoder is to generate new feature vectors that will reduce the loss of predicted gene class label, reduce the loss of predicted bag class label and at the same time, increase the loss of predicted domain class label. This will hopefully force the auto-encoder to generate domaininvariant features and hence realize the transfer of knowledge from the gene domain into the isoform domain. The new (encoded) feature vectors in the matrix x_f are then partitioned into encoded gene feature vectors x_s^\prime and encoded isoform feature vectors x'_{t} . Each former vector is mapped by the gene class label predictor to predict a label y_s' in the gene domain and we denote the weights in this mapping as w_s . Each latter vector is mapped by the isoform class label predictor to predict a label y'_t in the target domain and we denote the weights in this mapping as w_t . See Figure 1 for the detailed NN architecture.

We train the NN by following a five-fold cross-validation procedure in the isoform domain and use the annotated GO terms of genes to evaluate its performance, similar to (Eksi et al., 2013; Li et al., 2013; Panwar et al., 2016). The data is partitioned by genes instead of isoforms to avoid potential data leak, as done in (Panwar et al., 2016). Note that since isoforms from homologous genes of the human genome (i.e., paralogs) do not generally share similar expression profiles (Li et al., 2013), it is unlikely for them to cause data leak in expression-based prediction of isoforms as demonstrated in (Eksi et al., 2013). All data from the gene domain is alwavs applied to enable DA, but the single-isoform genes in the isoform domain are left out of training to avoid overfitting. Before the training is

started, the variable $y_t[i]$ for isoform i is initialized as follows:

$$y_t^0[i] = \begin{cases} 1, & \text{if } x_t \in X_T[i,j] = 1 \land Y_T[j] = 1) \\ 0, & \text{if } x_t \in X_T[i,j] = 1 \land Y_T[j] = 0) \end{cases}$$
 The model is then trained for each GO term separately. To take advan-

tage of the hierarchical structure of GO, we traverse GO starting from the leaf nodes and train the model on a parent node only after all its children have been considered. This allows the training for a parent node to benefit from the knowledge learned from its children, as sketched schematically in Figure S1 of the Supplementary Materials. as well as help make the predicted labels more consistent between parents and children.

The weights w_f, w_d, w_s, w_t are determined during training to mini-

The weights
$$w_f, w_d, w_s, w_t$$
 are determined during training to minimize the following objective function:
$$L(w_f, w_s, w_t, w_d) = \sum_{i=1,...,n,y_d[i]=0} L^i{}_s(w_f, w_s)$$

$$+\lambda_1 \sum_{i=1,\dots,m,y_d[i]=1} L^i{}_t(w_f,w_t) - \lambda_2 \sum_{i=1,\dots,n+m} L^i{}_d(w_f,w_d)$$
(2)

where $L^{i}{}_{s}$ denotes the loss in gene class label prediction at the ith gene, L^{i}_{t} the loss in bag class label prediction at the ith bag and L^{i}_{d} the loss in domain class label prediction at the ith gene or isoform (see Figure 1). More precisely, for a fixed gene (or bag or isoform/gene) i, these loss functions are:

$$\begin{split} L^i{}_s(w_f, w_s) &= -\{y_s[i] \log y_s'[i] + (1 - y_s[i]) \log(1 - y_s'[i])\} \\ L^i{}_t(w_f, w_t) &= -\{Y_T[i] \log Y_T'[i] + (1 - Y_T[i]) \log(1 - Y_T'[i])\} \\ L^i{}_d(w_f, w_d) &= -\{y_d[i] \log y_d'[i] + (1 - y_d[i]) \log(1 - y_d'[i])\} \end{split}$$

We now show how the loss function $L_t[i]$ is derived. Given the predicted class labels of the isoforms in bag i, we can estimate the class label of the bag using the method proposed in (Wang et al., 2015) for dealing with multiple instance loss as shown in equation 4. Clearly, if at least one instance of the bag is positive, the bag will be predicted as positive; otherwise, it will be considered as negative.

$$Y'_{T}[i] = 1 - \prod_{j \in \text{bag } i} (1 - y'_{t}[j])$$
 (4)

$$y'_t[j] = \frac{1}{1 + e^{-w_t \cdot x'_t[j]}}$$
 (5) $x'_t[j] = \frac{1}{1 + e^{-w_f(t) \cdot x_t[j]}}$

Here, i denotes a bag and j an isoform. The predicted isoform class label $y'_{t}[j]$ for isoform j is calculated by the sigmoid function in equation 5. The encoded feature vector of isoform j, $x'_t[j]$, is calculated by another sigmoid function given in equation 6. The weights $w_f(t)$ represent the part of w_f derived from the isoform data. The other part of w_f , denoted as $w_f(s)$, represents the weights derived from the gene data. Similar sigmoid functions are used to derive the values of y_s' and y_d' used in equation

As mentioned above, we would like to seek the values of w_f, w_s, w_t, w_d to achieve a saddle point of equation 2 such that $\hat{w}_f, \hat{w}_s, \hat{w}_t = arg \min_{w_f, w_s, w_t} L(w_f, w_s, w_t, \hat{w}_d)$ (7)

$$\hat{w}_d = \arg\max_{w_d} L(\hat{w}_f, \hat{w}_s, \hat{w}_t, w_d)$$

At the saddle point, the weights \boldsymbol{w}_d of the domain label predictor maximize the loss in domain classification while the weights w_s and w_t of the class label predictors minimize the loss in functional prediction in both domains. The feature mapping weights w_f help minimize the class label prediction loss while maximizing the domain classification loss. A saddle point of equation 7 can be found as a stationary point by using the following stochastic updates as suggested in (Ganin and Lempitsky,

$$\begin{split} w_f \leftarrow w_f - \alpha (\frac{\partial L_s}{\partial w_f(s)} + \lambda_1 \frac{\partial L_t}{\partial w_f(t)} - \lambda_2 \frac{\partial L_d}{\partial w_f}) \\ w_s \leftarrow w_s - \alpha (\frac{\partial L_s}{\partial w_s}) \\ w_t \leftarrow w_t - \alpha (\frac{\partial L_t}{\partial w_t}) \\ w_d \leftarrow w_d - \alpha (\frac{\partial L_d}{\partial w_d}) \end{split}$$

where the parameters λ_1 and λ_2 control the relative contributions of the predictors during learning and α denotes the learning rate in this process.

3 Experimental evaluation

In this section, we describe in detail how to choose the key parameters in the NN model, how the test data is collected, and how the computational experiments are performed as well as what are their results.

3.1 The deep NN parameters

DeepIsoFun has been implemented in Caffe (Jia et al., 2014). In our NN architecture, the auto-encoder consists of two fully-connected layers to extract common features of the gene and isoform domains. The first fullyconnected layer consists of 600 neurons and the second fully-connected layer consists of 200 neurons. The number of hidden layers and size of each layer (i.e., number of neurons in the layer) were optimized by a standard grid search method (Bergstra et al., 2011; Bergstra and Bengio, 2012). The gene class label predictor and isoform class label predictor modules are both output layers, and hence have only a single output neuron each. The domain label predictor module uses a fully connected layer with 300 neurons and an output layer with a domain output neuron. We used a standard stochastic gradient descent optimization method to minimize the training error as represented by the loss function given in equation 2 that involves two parameters λ_1 and λ_2 . Both parameters were tuned experimentally by following suggestions in the literature (Bergstra and Bengio, 2012; Snoek et al., 2012). In particular, the parameter λ_2 weighting the contribution from domain label prediction was set by using the following formula: $\lambda_2=\frac{2}{1+e^{-10p}}-1$

$$\lambda_2 = \frac{2}{1 + e^{-10p}} - 1$$

By adjusting $p \in [0,1]$, we gradually tuned λ_2 so that noise from the

domain label predictor is minimized at early training stages. The isoform domain data was partitioned in the five-fold cross-validation procedure to produce the training and test data. The batch size used in stochastic training of the NN model was 200. In other words, 200 source samples (genes) and 200 target samples (isoforms) are merged to create a batch. At the initial training stage, the leaning rate was set as $\alpha=0.001$. As training progresses, we update the learning rate by using the standard step decay procedure (Sutskever et al., 2013) implemented in Caffe. We also checked if the learning was diverging (e.g., very large loss values were observed), and dropped the initial learning rate by a factor 10 until convergence has been achieved.

3.2 Collection of datasets

Manually reviewed mRNA isoform sequences and gene sequences of human were collected from the NCBI RefSeq (Pruitt et al., 2005). To collect the expression profiles of these isoforms, we took an initial set of 4643 RNA-Seq experiments from the NCBI SRA database (Leinonen et al., 2010), and selected datasets with 50 million to 100 million reads. These experiments represented different physiological and cell conditions but were not involved in population studies. Such a diverse set of expression data may reflect many complex characteristics of the isoforms. The tool Kallisto (Bray et al., 2016) with Sleuth (Pimentel et al., 2016) was used to generate isoform expression data measured in TPMs (Transcripts Per Million). The expression level of a gene in a dataset was estimated by summing up the expression levels of all its isoforms. Experiments with the pseudo-alignment ratio less than 0.7 were discarded to ensure data quality. We also filtered out poorly covered genes and their corresponding isoforms in these experiments. Finally, the expression data of 19532 genes and 47393 isoforms from 1735 RNA-Seq experiments formed our first dataset (simply called Dataset#1). Out of these genes, 9039 have only one isoform and are called single-isoform genes (SIGs) and 10313 have more than one isoform and are called multiple-isoform genes (MIGs). The distribution of isoforms over genes is shown in Figure S2 of the Supplementary Materials. UniProt genes were mapped to RefSeq genes by using the UniProt ID mapping file. The UniProt GO database was used to annotate the functions of each RefSeq gene, where GO functions inferred from electronic annotation (IEA) evidence code were discarded as done in (Li et al., 2013). In other words, only manually curated functions were used for the final annotation. The number of genes associated with a GO term is referred to as the GO term size. Intuitively, GO terms with small sizes are computationally difficult to learn since its data is highly skewed (i.e., mostly negative). In particular, it was assumed in (Eksi et al., 2013) that a GO term with size less than 5 might be very specific to certain genes and thus not very useful in the cross-validation training procedure. We hence did not consider such infrequent GO terms in our experiments. The basic version of GO was used to generate the parent-child relationship between GO terms (Ashburner et al., 2000). Out of all 44612 GO terms, 14563 appear in human annotations. After the above filtration, 4272 GO terms were kept for our experimental evaluation work. In addition to Dataset#1, we also used the datasets with their respective GO annotations introduced in (Eksi et al., 2013) and (Li et al., 2013) (called Dataset#2 and Dataset#3, resp.) to ensure our comparison results are unbiased, where Dataset#2 was generated from 116 SRA mouse studies consisting of 365 experiments and Dataset#3 was generated from 29 SRA human studies consisting of 455 experiments with the requirement that each study had more than 6 experiments.

3.3 Experimental results

Since isoform functions are generally unavailable, we evaluated the performance of DeepIsoFun using gene level functional annotations by considering SIGs and MIGs either together or separately, as done similarly in (Eksi et al., 2013; Li et al., 2013). Because each SIG contains only one isoform, its functional annotation can be used to directly validate the

predicted functions of the involved isoform. For a MIG, we can only check if the set of the predicted functions of its isoforms is consistent with its annotated GO terms (Eksi et al., 2013). We also estimated the functional divergence achieved by the isoforms of the same gene by calculating the semantic dissimilarity for each of the three main branches of GO (i.e., CC, BP and MF). The tool GOssTo (Caniza et al., 2014) was used to perform this estimation because it was able to take into account the hierarchical structure of GO. Moreover, we analyzed how the DA technique really helped the performance of our method, how the size of a GO term impacted the performance and the correlation between expression similarity and predicted function similarity for isoforms. Finally, we compared our method with the methods in (Eksi et al., 2013; Li et al., 2013; Luo et al., 2017; Panwar et al., 2016) in terms of AUC and AUPRC against specific baselines by focusing on a small set of GO terms (i.e., GO Slim with 117 terms) that have been widely used in the literature (Ashburner et al., 2000). Here, a baseline represents the performance of a random (untrained) classifier (Saito and Rehmsmeier, 2015). While the baseline in an AUC estimation is always 0.5 (Fawcett, 2006; Metz, 1978), the baseline in an AUPRC estimation depends on data imbalance and equals the proportion of positive instances (Saito and Rehmsmeier, 2015). The latter measure is known to be more suitable for imbalanced data. Note that for highly imbalanced data (like ours), AUPRC values are often quite low (Davis and Goadrich, 2006; Saito and Rehmsmeier, 2015). However, we may still use them to compare the relative performance of different methods on various datasets, taking into account actual baselines.

3.3.1 Performance on the three main branches of GO

Since the three main branches carry very different meanings in gene functions and are often treated separately in the literature, we compared the performance of DeepIsoFun on them. Out of the 4272 GO terms, 699 belong to CC, 2178 BP and 1395 MF. The distributions of GO term sizes on the three branches are similar. The average AUC values on BP, CC and MF are 0.735, 0.728 and 0.722, respectively, (see Figure 2a) and the average AUPRC values are 0.301, 0.279 and 0.294, respectively, (see Figure 2b). This robust performance of DeepIsoFun on the three main branches of GO shows that the terms on the branches probably follow similar distributions (as already observed on the distributions of their sizes).

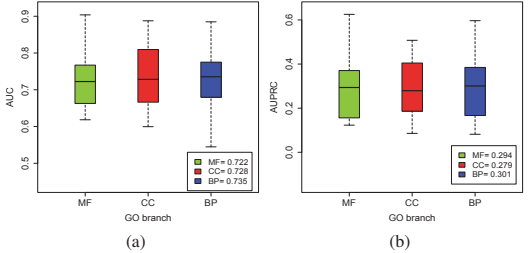
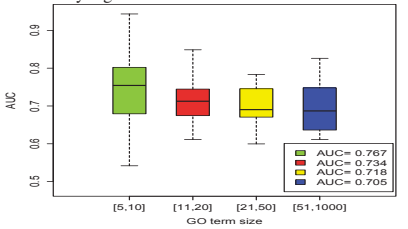


Figure 2: Comparison of performance on the three main branches of GO. (a) The average AUC values on the three branches. (b) The average AUPRC values on the three branches.

3.3.2 Impact of the size of a GO term on performance

Some GO terms are very specific to certain genes while the others are more general. To test how the size (or popularity) of a GO term would impact the performance of DeepIsoFun, we divided the GO terms into four groups based on size. The four groups consist of GO terms of sizes in ranges [5-10], [11-20], [21-50], and [51-1000], respectively. The performance of DeepIsoFun on these groups is given in Figure 3a. DeepIsoFun performed better on GO terms with smaller sizes in general. This pattern seems to contradict intuition, but it is consistent with the findings in (Li et al., 2013) and can perhaps be explained by the large the amount of (annotation) noise in large size GO terms. To confirm this, we further analyzed the correlation between expression similarity and functional similarity with

respect to GO terms in each of the four groups. The results in Figure S3 of the Supplementary Materials suggest that the correlation decreases as the GO term size increases. The weak correlations shown in the figure also partially explain why the AUC and AUPRC values obtained in Figure 2 are not very high.



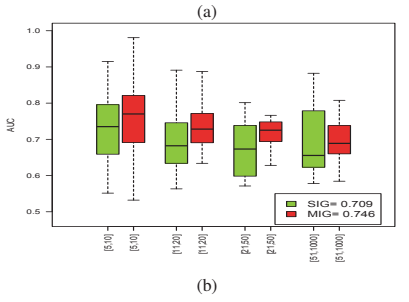


Figure 3: Comparison of AUCs achieved in four groups of GO terms from CC with different sizes. The four groups contain terms with sizes in ranges [5-10], [11-20], [21-75], and [76-1000], respectively. (a) The average AUC values achieved by the terms in the four groups are 0.767, 0.734, 0.718, and 0.705, respectively. The plot shows that generally as the size of a GO term increases, its achieved AUC actually decreases. (b) DeepIsoFun consistently performed better on MIGs over SIGs. The average AUC values on MIGs achieved in the four groups are 0.79, 0.748, 0.745, and 0.709, respectively. the average AUC values on SIGs achieved by in four groups are 0.755, 0.702, 0.693, and 0.675, respectively.

3.3.3 Performance on MIGs vs SIGs

In the previous section, we considered the performance of DeepIsoFun on all genes, including both SIGs and MIGs. Since our ultimate goal is to dissect functions of different functions of the same gene, we would like to compare the performance on MIGs with that on SIGs in this subsection. As shown in Figure 3b, the performance increases as term size decreases. Moreover, the performance on MIGs achieved in these groups are consistently better than the performance on SIGs. More precisely, the performance on MIGs was 14%, 23%, 27%, and 19% better (against the baseline 0.5) than that on SIGs in the four groups, respectively. Hence, DeepIsoFun was more effective in predicting functions for genes with multiple isoforms than genes with a single isoform, probably because of the functional diversity usually acquired by the former. Another plausible cause is that, since most (95%) human genes are expected to be MIGs. many SIGs could represent poorly annotated genes that have large numbers of undiscovered isoforms. Therefore, we also analyzed the performance of DeepIsoFun on MIGs with a certain number of isoforms. As shown in Figure S4 of the Supplementary Materials, the AUC performance of DeepIsoFun increases (slightly) as more isoforms are found in a MIG.

3.3.4 Dissimilarity among the predicted functions of isoforms

Since our ultimate goal is to dissect the functions of isoforms, we estimate the functional divergence of the isoforms of the same gene. For each GO term, the gene-wise method simGIC of GOssTo (Caniza *et al.*, 2014; Pesquita *et al.*, 2007) was used to calculate the semantic similarity score in the range of [0,1] for each gene based on the predicted functions of

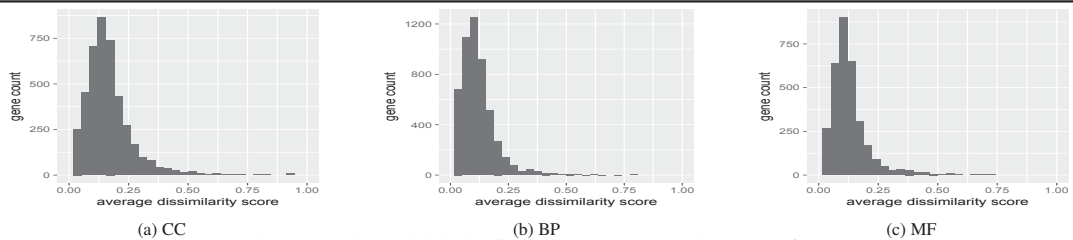


Figure 4: Functional dissimilarity distributions on the three main branches of GO.

its isoforms. The dissimilarity score was simply defined as one minus the similarity score (Li et al., 2013). Again, the three main branches of GO (i.e., CC, BP and MF) were considered separately. Out of the 10313 MIGs, 4310 genes appear in CC, 5224 appear in BP and 3217 appear in MF (a gene may contain functions from multiple branches). For each branch, the functional divergence of a gene is calculated as the average dissimilarity scores over all terms on the branch. Figure 4 shows the distribution of functional dissimilarity scores among the isoforms of each gene. As observed in the literature (Li et al., 2013; Schlicker et al., 2006), many genes exhibited low average dissimilarity scores. More precisely, about 24% (1033) of the genes that appear in CC showed average dissimilarity scores less than 0.1. For BP and MF, this percentage rose to 46% (2405 genes) and 39% (1280 genes). On the other hand, about 7%, 3% and 4% of the genes have average dissimilarity scores greater than 0.3 on the three branches, respectively. These results are consistent with the fact that the isoforms of the same genes have very similar sequences, which lead them to perform mostly similar functions, but some isoforms may still have very different functions due to large changes in promoters and/or composition

3.3.5 Effectiveness of domain adaptation

A main novelty in DeepIsoFun is the use of DA (domain adaptation) to create labeled training data and transfer knowledge from the gene domain to the isoform domain. To test the effectiveness of DA in the experiments, we compared DeepIsoFun with a version without DA where the third part of the objective function in equation 2 is disabled. Compared with the average AUC of 0.695 achieved by the restricted DeepIsoFun without DA, DeepIsoFun with DA performed 18% better against the baseline 0.5 as shown in Figure 5. We then further compared the two versions on the four GO term groups based on term sizes and found that the DA technique always made a significant difference. More specifically, it helped DeepIsoFun to achieve 19%, 19%, 17%, and 20% better AUC (against the baseline 0.5) in the four groups, respectively.

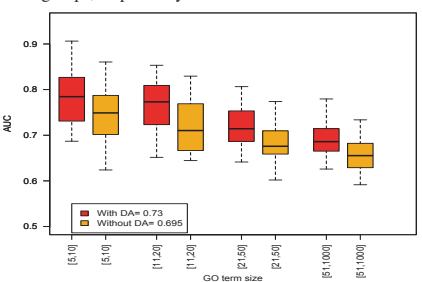


Figure 5: Comparison of AUCs achieved in the four groups of GO terms by DeepIsoFun with and without the DA technique. The average AUC value achieved by DeepIsoFun with DA in all four groups is 0.730 and the corresponding AUC achieved by DeepIsoFun without DA is 0.695. The benefit of DA is also clearly shown in the comparison over individual groups.

We also tested if the DA technique was actually able to mix the two domains (so knowledge can be transferred). The plots in Supplementary Figure S5 made by using t-SNE (Maaten and Hinton, 2008) show clearly that the extracted features from the two domains became indistinguishable with the help of DA. This makes it possible to transfer knowledge (*i.e.*, the relationship between expression profiles and functions) from the gene domain to the isoform domain and is a key to the improved performance of DeepIsoFun.

3.3.6 Correlation between expression similarity and the similarity of predicted functions

Given the difficulty in testing the performance of DeepIsoFun directly due to the lack of isoform function benchmark, we tested how the predicted isoform functions are correlated with their expression profiles. After all, this was the original hypothesis behind the design of DeepIsoFun. We performed a hierarchical clustering of the isoforms based on the expression data and Euclidean distance by using a standard tool (hclust) in the R Stats package. Eight clusters were defined from the clustering tree using the same tool. Then, the average distance between the expression profiles of the isoforms within each cluster was calculated and normalized to the range of [0,1]. The same thing was done to estimate the average distance between the predicted GO terms of the isoforms within each cluster. The distributions of the average distances over the clusters are shown in Figure 6. Clearly, isoforms with similar expression profiles resulted in similar predicted functions.

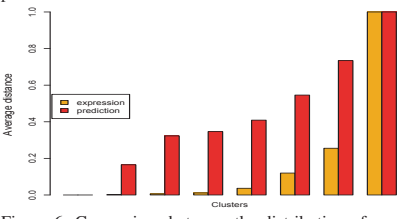


Figure 6: Comparison between the distribution of expression similarity and the distribution of similarity concerning predicted functions. The plot shows a clear positive correlation between the two distributions.

3.3.7 Comparison with the existing methods

We compared the performance of DeepIsoFun with three existing methods, iterative Multiple Instance Label Propagation (iMILP) (Li et al., 2013), Multiple Instance SVM (mi-SVM) (Eksi et al., 2013; Panwar et al., 2016) and the Weighted Logistic Regression Method (WLRM) (Luo {\it et al.}, 2017). Here, iMILP is the iterative version of MILP where a feature selection wrapper method is run over MILP to achieve better performance (Li et al., 2013). For completeness, we will also included MILP in the comparison. Note that WLRM was compared in (Luo et al., 2017) with two recent methods for solving MIL, namely miFV (Wei et al., 2014) and miVLAD (Wei et al., 2017), and found to perform better in the prediction of isoform functions. In addition to Dataset#1 analyzed above, we also considered the two expression datasets introduced in (Eksi et al., 2013; Li et al., 2013), Dataset#2 and Dataset#3, respectively. Since mi-SVM and WLRM follow a 2-class classification framework but MILP/iMILP adapt a 3-class classification framework, different benchmarks were used to create functional labels for training and testing in (Eksi et al., 2013; Li et al., 2013; Luo et al., 2017; Panwar et al., 2016). In a 2-class classification framework, an isoform is classified as either positive or negative with respect to each GO term, while in a 3-class classification framework, an isoform

is classified as either positive, negative or unknown. Hence, we present the comparison between DeepIsoFun and MILP/iMILP in Table 1 and the comparison among DeepIsoFun, mi-SVM and WLRM in Table 2. Note that the values in the two tables are not directly comparable. On all three datasets, DeepIsoFun performed significantly better than the other methods. The average AUC values achieved by DeepIsoFun on all three datasets are 0.742, 0.734 and 0.720 with respect to the first benchmark (Table 1), and 0.735, 0.729 and 0.704 with respect to the second benchmark (Table 1). The corresponding values of AUPRC are 0.368 (baseline 0.1), 0.270 (baseline 0.08) and 0.331 (baseline 0.11) with respect to the first benchmark, and 0.292 (baseline 0.1), 0.246 (baseline 0.08) and 0.234 $\,$ (baseline 0.11) with respect to the second benchmark. Note that although the AUPRC values are lower, they still represent quite decent performance when compared to the baseline values. The best performance achieved on Dataset#1 is perhaps due to the quality of data (since it was collected most recently and processed with updated tools) and its diversity across different tissue conditions. On this dataset, compared to iMILP, MILP, mi-SVM and WLRM, the AUC of DeepIsoFun increased 64%, 102%, 31%, and 23% against the baseline 0.5, respectively. Similarly, on Dataset#2 (or Dataset#3), the improvements are 73%, 216%, 37%, and 45% (or 26%, 450%, 43%, and 24%) against the baseline, respectively. Since our labeled data was imbalanced, we also compared the performance in AUPRC and observed similar improvements. On Dataset#1 (Dataset#2 and Dataset#3). DeepIsoFun performed 59% (29% and 41%, resp.) better than mi-SVM in AUPRC against respective baselines, 11% (23% and 10%, resp.) better than iMILP, 57% (32% and 20%, resp.) better than MILP, and 63% (62% and 85%, resp.) better than WLRM. We think that these significant improvements in performance over the existing methods on several human and mouse datasets demonstrate the success of the DA technique as well as the power of deep learning.

Table 1. Comparison between DeepIsoFun and MILP/iMILP on different expression datasets in terms of AUC and AUPRC values. Dataset#1 was generated from 1735 RNA-Seq experiments by using Kallisto (Bray et al., 2016). Dataset#2 and Dataset#3 were obtained from (Eksi et al., 2013) and (Li et al., 2013), respectively. The benchmark positive and negative instances of each GO term used in testing were defined by following the procedure in (Li et al., 2013). The unlabeled instances were ignored in testing. Both Dataset#1 and Dataset#2 were divided based on read length to create different "study groups". There are 24, 24 and 29 study groups in Dataset#1, Dataset#2 and Dataset#3, respectively. On the average, each study group consists of 71, 16 and 17 SRA experiments in Dataset#1, Dataset#3, respectively. As done in (Li et al., 2013), a selection algorithm was employed by iMILP to choose a subset of study groups on each dataset optimize its performance.

	A	AUC		AUPRC			
Method Dataset	DeepIsoFun	MILP	iMILP	DeepIsoFun	MILP	iMILP	
Dataset#1	0.742	0.620	0.648	0.368	0.271	0.342	
Dataset#2	0.734	0.574	0.635	0.270	0.224	0.235	
Dataset#3	0.720	0.540	0.674	0.331	0.294	0.311	

Table 2. Comparison among DeepIsoFun, mi-SVM and WLRM on different expression datasets in terms of AUC and AUPRC values. The benchmark positive and negative instances of each GO term used in testing were defined by following the procedure in (Eksi et al., 2013).

	AUC			AUPRC		
Method Dataset	DeepIsoFun	mi-SVM	WLRM	DeepIsoFun	mi-SVM	WLRM
Dataset#1	0.735	0.679	0.691	0.292	0.221	0.218
Dataset#2	0.729	0.667	0.658	0.246	0.209	0.182
Dataset#3	0.704	0.643	0.664	0.234	0.198	0.177

Some comparisons of the methods in terms of divergence of predicted isoform functions and time efficiency are given in the Supplementary Materials (Figure S6 and Table S1). We also compared the performance of the

methods on two additional datasets concerning Arabidopsis thaliana and Drosophila melanogaster (i.e., fruit fly) and summarize the comparison results in Tables S2 and S3 of the Supplementary Materials. As the tables show, DeepIsoFun consistently performed better than the other methods in both AUC and AUPRC. The performance of the methods on all five datasets with respect to different GO term sizes is given in Tables S4 and S5.

3.3.8 Validation of some predicted isoform functions

As mentioned before, there has been little systematic study on isoform functions in the literature, and not many specific experimentally-verified functions of isoforms have been reported. Some of the reported functions concern differential regulatory behaviors of isoforms in important processes such as the 'regulation of apoptosis process' (GO:0042981). Apoptosis refers to programmed cell death. This GO term has two children with opposite functions, i.e., the 'positive regulation of apoptosis process' or pro-apoptosis (GO:0043065) and the 'negative regulation of apoptosis process' or anti-apoptosis (GO:0043066). For MIGs with both pro-apoptosis and anti-apoptosis functions, it would be interesting to know if it has some isoforms that are pro-apoptosis but not anti-apoptosis and some other isoforms that are anti-apoptosis but not pro-apoptosis. In other words, we would like to know if the pro- and anti-apoptosis functions of the gene are differentiated among its isoforms. To investigate such MIGs, we searched for all genes that have multiple isoforms and are annotated with both pro-apoptosis and anti-apoptosis functions. Totally, 18 such genes were found (see Table S6 in the Supplementary Materials). The number of isoforms in each of these genes ranges from 2 to 17. Tables S6, S7, S8, and S9 in the Supplementary Materials show the performance of DeepIsoFun, iMILP, mi-SVM, and WLRM, respectively, in predicting the apoptosis regulatory, pro-apoptosis and anti-apoptosis functions, measured at the gene level. DeepIsoFun was able to predict the apoptosis regulatory function for the isoforms of 17 out of the 18 genes (94.4% recall), the pro-apoptosis function for the isoforms of 13 genes (72.2% recall) and the anti-apoptosis function for the isoforms of 14 genes (77.7% recall). In contrast, iMILP achieved recalls 77.7%, 55.6% and 61.1%, mi-SVM achieved recalls 83.3%, 66.7% and 61.1% and WLRM achieved recalls 77.7%, 61.1% and 72.2% in predicting the three functions, respectively. Futhermore, the tables show that DeepIsoFun was able to differentiate the pro- and anti-apoptosis functions among isoforms for 8 of the 18 genes while iMILP, mi-SVM and WLRM were only able to do it for 5, 4 and 3 genes, respectively. Although we do not know exactly how many of these genes have differentiated pro- and anti-apoptosis functions among their isoforms, it is perhaps reasonable to conjecture that most of these genes do possess this property.

4 Discussion

Although DeepIsoFun achieved significant improvement over the existing methods in isoform function prediction, its performance as measured by AUC and AUPRC in our experiments still remained less than desirable. The prediction of isoform functions is challenging not only because of the lack of labeled training data (i.e., specific functions are known for very few isoforms) and noisy GO annotation, but also because the data is very imbalanced. That is, most GO terms are only associated with a small number of genes and hence the negative examples are far more than the positive examples. This makes the situation especially bad when the performance is measured in AUPRC since the number of false positive examples tends to be high and thus the precision tends to be low. We dealt with the problem by leaving out infrequent GO terms that are associated with fewer than five genes, although such terms often represent specific functions and could be biologically the most relevant. On the other hand, most functions of genes are yet to be discovered. Hence, three-class classification was proposed in (Li et al., 2013) as a way to address the data imbalance issue. However, such an approach often leads to conservative predictions and may fail to

predict many isoform specific functions. We plan to study machine learning (including unsupervised learning) techniques that can help produce meaningful predictions for infrequent GO terms.

Another challenge we faced was the heterogeneity of the expression data. While a large dataset covering many tissues and conditions (such as Dataset#1) provides rich information about isoform functions, it also contains a lot of noise that makes the extraction of informative features difficult. (Li et al., 2013) solved this problem by using an elaborate search procedure to identify the best subset of RNA-Seq experiments in the input data. However, the search consumes a lot of time, especially when the number of input RNA-Seq experiments is large. We plan to apply Deep-IsoFun to tissue-specific data to see how its performance will be affected as well as if some tissue-specific isoform functions can be discovered.

Acknowledgment

We would like to thank the authors of (Eksi *et al.*, 2013; Li *et al.*, 2013; Lu *et al.*, 2017) for sharing their data and code with us. The research was partially supported by National Science Foundation grant IIS-1646333 and the Natural Science Foundation of China grant 61772197.

References

- Ajakan, H. et al (2014). Domain-adversarial neural networks. arXiv preprint arXiv:1412.4446.
- Andrews, S. et al (2003). Support vector machines for multiple-instance learning. In Advances in neural information processing systems, pages 577–584.
- Ashburner, M. et al (2000). Gene ontology: tool for the unification of biology. *Nature* genetics. **25**(1), 25–29.
- Barrell, D. et al (2008). The goa database in 2009âŁ"an integrated gene ontology annotation resource. Nucleic acids research, 37(suppl_1), D396–D403.
- Barutcuoglu, Z. et al (2006). Hierarchical multi-label prediction of gene function. *Bioinformatics*, **22**(7), 830–836.
- Brongsmants, 22(7), 630-630.
 Bergstra, J.S. et al (2012). Random search for hyper-parameter optimization. *Journal of Machine Learning Research*, 13(Feb), 281–305.
- Bergstra, J.S. et al (2011). Algorithms for hyper-parameter optimization. In Advances in Neural Information Processing Systems, pages 2546–2554.
- Bouillet, P. et al (2009). Cd95, bim and t cell homeostasis. *Nature Reviews Immunology*, **9**(7), 514–519.
- Bray, N.L. et al (2016). Near-optimal probabilistic rna-seq quantification. Nature
- biotechnology, 34(5), 525-527.

 Caniza, H. et al (2014). Gossto: a stand-alone application and a web tool for
- calculating semantic similarities on the gene ontology. *Bioinformatics*, **30**(15), 2235–2236.

 Consortium, G.O. et al (2004). The gene ontology (go) database and informatics
- resource. *Nucleic acids research*, **32**(suppl 1), D258–D261.
- Davis, J. et al (2006). The relationship between precision-recall and roc curves. In Proceedings of the 23rd international conference on Machine learning, pages 23 240, ACM.
- Dietterich, T.G. et al (1997). Solving the multiple instance problem with axis-parallel rectangles. *Artificial intelligence*, **89**(1), 31–71.

 Eksi, R. et al (2013). Systematically differentiating functions for alternatively spliced
- Eksi, K. et al (2013). Systematically differentiating functions for alternatively spliced isoforms through integrating ma-seq data. *PLoS computational biology*, 9(11), e1003314.
- Fawcett, T. (2006). An introduction to roc analysis. *Pattern recognition letters*, **27**(8), 861–874.
- Gallego-Paez, L. et al (2017). Alternative splicing: the pledge, the turn, and the prestige. Human Genetics, pages 1–28.
- Ganin, Y. et al (2015). Unsupervised domain adaptation by backpropagation. In International Conference on Machine Learning, pages 1180–1189.
- Gueroussov, S. et al (2015). An alternative splicing event amplifies evolutionary differences between vertebrates. Science, 349(6250), 868–873.
- Himeji, D. et al (2002). Characterization of caspase-8l: a novel isoform of caspase-8 that behaves as an inhibitor of the caspase cascade. Blood, 99(11), 4070–4078.
- Jia, Y. et al (2014). Caffe: Convolutional architecture for fast feature embedding. In Proceedings of the 22nd ACM international conference on Multimedia, pages 675–678. ACM.
- Leinonen, R. et al (2010). The sequence read archive. *Nucleic acids research*, **39**(suppl_1), D19–D21.
- Li, H.D. et al (2015). Misomine: a genome-scale high-resolution data portal of expression, function and networks at the splice isoform level in the mouse. *Database*, 2015, bav045.

- Li, W. et al (2013). High-resolution functional annotation of human transcriptome: predicting isoform functions by a novel multiple instance-based label propagation method. *Nucleic acids research*, 42(6), e39–e39.
- Long, M. et al (2015). Learning transferable features with deep adaptation networks. In *International Conference on Machine Learning*, pages 97–105.
- Luo, T. et al (2017). Functional annotation of human protein coding isoforms via non-convex multi-instance learning. In Proceedings of the 23rd ACM SIGKDD International Conference on Knowledge Discovery and Data Mining, pages 345– 354. ACM.
- Maaten, L.v.d. et al (2008). Visualizing data using t-sne. *Journal of Machine Learning Research*, **9**(Nov), 2579–2605.
- Mazurek, S. et al (2005). Pyruvate kinase type m2 and its role in tumor growth and spreading. In Seminars in cancer biology, volume 15, pages 300–308. Elsevier.
- Melamud, E. et al (2009). Stochastic noise in splicing machinery. Nucleic acids research, 37(14), 4873–4886.
- Metz, C.E. (1978). Basic principles of roc analysis. In Seminars in nuclear medicine, volume 8, pages 283–298. Elsevier.
- Mi, H. et al (2012). Panther in 2013: modeling the evolution of gene function, and other gene attributes, in the context of phylogenetic trees. *Nucleic acids research*, **41**(D1), D377–D386.
- Mittendorf, K.F. et al (2012). Tailoring of membrane proteins by alternative splicing of pre-mrna. *Biochemistry*, 51(28), 5541.
- Oberwinkler, J. et al (2005). Alternative splicing switches the divalent cation selectivity of trpm3 channels. *Journal of Biological Chemistry*, 280(23), 22540–22548.
- Pan, Q. et al (2008). Deep surveying of alternative splicing complexity in the human transcriptome by high-throughput sequencing. *Nature genetics*, **40**(12), 1413-15.
- Pan, S.J. et al (2011). Domain adaptation via transfer component analysis. *IEEE Transactions on Neural Networks*, 22(2), 199–210.
- Panwar, B. et al (2016). Genome-wide functional annotation of human protein-coding splice variants using multiple instance learning. *Journal of proteome research*, 15(6), 1747–1753.
- Pesquita, C. et al (2007). Evaluating go-based semantic similarity measures. In *Proc.* 10th Annual Bio-Ontologies Meeting, volume 37, page 38.
- Pickrell, J.K. et al (2010). Noisy splicing drives mrna isoform diversity in human cells. *PLoS genetics*, 6(12), e1001236.
- Pimentel, H.J. et al (2016). Differential analysis of rna-seq incorporating quantification uncertainty. biorxiv.
- Pruitt, K.D. et al (2005). Ncbi reference sequence (refseq): a curated non-redundant sequence database of genomes, transcripts and proteins. *Nucleic acids research*,
- 33(suppl_1), D501–D504.

 Revil, T. et al (2007). Protein kinase c-dependent control of bcl-x alternative splicing.

 Molecular and cellular biology, 27(24), 8431–8441.
- Saito, T. et al (2015). The precision-recall plot is more informative than the roc plot when evaluating binary classifiers on imbalanced datasets. *PloS one*, **10**(3),
- Schietgat, L. et al (2010). Predicting gene function using hierarchical multi-label decision tree ensembles. BMC bioinformatics, 11(1), 2.
- Schlicker, A. et al (2006). A new measure for functional similarity of gene products based on gene ontology. $BMC\ bioinformatics$, 7(1), 302.
- Snoek, J. et al (2012). Practical bayesian optimization of machine learning algo-
- rithms. In Advances in neural information processing systems, pages 2951–2959. Sutskever, I. et al (2013). On the importance of initialization and momentum in deep
- learning. In International conference on machine learning, pages 1139–1147.
- Tzeng, E. et al (2014). Deep domain confusion: Maximizing for domain invariance. arXiv preprint arXiv:1412.3474.
- Vázquez, Á.V. et al (2011). Two proteins with different functions are derived from the klhem13 gene. *Eukaryotic cell*, **10**(10), 1331–1339.
- Végran, F. et al (2006). Overexpression of caspase-3s splice variant in locally advanced breast carcinoma is associated with poor response to neoadjuvant chemotherapy. Clinical cancer research, 12(19), 5794–5800.
- Vinayagam, A. et al (2004). Applying support vector machines for gene ontology based gene function prediction. BMC bioinformatics, 5(1), 116.
- Wang, E.T. et al (2008). Alternative isoform regulation in human tissue transcrip-
- tomes. *Nature*, **456**(7221), 470–476.
 Wang, J. et al (2017). Multiple-instance learning via an rbf kernel-based extreme
- learning machine. Journal of Intelligent Systems, 26(1), 185–195.
- Wang, X. et al (2015). Relaxed multiple-instance svm with application to object discovery. In Proceedings of the IEEE International Conference on Computer Vision, pages 1224–1232.
- Wei, X.S. et al (2014). Scalable multi-instance learning. In *Data Mining (ICDM)*, 2014 IEEE International Conference on, pages 1037–1042. IEEE.
- Wei, X.S. et al (2017). Scalable algorithms for multi-instance learning. IEEE transactions on neural networks and learning systems, 28(4), 975–987.
- Yang, J. et al (2015). The i-tasser suite: protein structure and function prediction. Nature methods, 12(1), 7–8.